Journal of Harbin Engineering University
ISSN: 1006-7043

Vol 45 No. 10
October 2024

Mechanical and Rheological Study of Reduced Graphene Oxide Filled Thermoplastic Polyester Elastomer Nanocomposites

Gyanesh Katiyar[1], Kavita Srivastava[2], Dr. Deepak Srivastava[3], Dr. Arun Maithani[4]

[1]Department of Plastic Technology, School of Chemical Technology, H B Technical University, Kanpur – 208 002 (U.P.), India.

[2]Department of Chemistry, V S S D College, Kanpur – 208 002 (U.P.), India.

[3]Department of Plastic Technology, School of Chemical Technology, H B Technical University, Kanpur – 208 002 (U.P.), India.

[4]Department of Paint Technology, School of Chemical Technology, H B Technical University, Kanpur – 208 002 (U.P.), India.

Email: Katiyar.g@gmail.com

Abstract

The study highlights the impact of incorporating reduced graphene oxide Nano sheets (RGO) into thermoplastic polyester elastomer (TPEE) composites of various compositions such as 0.5%,1.0%and 1.5%. The addition of RGO improves the modulus, yield strength, and tensile strength of TPEE. This indicates that RGO act as effective reinforcements in the composite material. Surface functionalization of RGO further enhances its reinforcing effect. This is attributed to improved interfacial interactions between the RGO and the TPEE matrix. Incorporating RGO increases the elongation levels of TPEE, suggesting enhanced elastoplastic and viscoelasticity. This is explained by the formation of a 'ball bearing' structure, where the discrete hard poly (butylene terephthalate) domains of TPEE enrich the surface of RGO. This structure allows for increased deformation ability of the soft continuous poly (tetramethylene glycol) of TPEE during large-scale deformation. Here, the impeding effect of RGO on the deformation of TPEE chain coils plays a dominant role. Overall, the study provides valuable insights into the structural design and control of RGO-filled thermoplastic elastomer composites, particularly regarding mechanical properties, deformation behavior, and the role of surface functionalization. These findings could inform the development of advanced materials with tailored properties for various applications.

Keywords: Thermoplastic Elastomer (TPEE), Graphene oxide (RGO), Mechanical properties.

Introduction

A relatively recent addition to the thermoplastic elastomer (TPEE) family, thermoplastic polyester elastomer (TPEE) was created for use in athletic goods, automotive, fluid power, and electronics [1]. Its typical composition consists of amorphous polyether, such as poly-tetramethylene ether glycol terephthalate), poly (alkylene glycol), poly (ethylene oxide), or poly (tetramethylene oxide), as the soft segment and crystalline polyester, such as poly (butylene terephthalate), poly (ethylene terephthalate), or poly (trimethylene terephthalate) as the hard segments [2,3]. Similar to other TPE family members, TPEE's soft amorphous domains show Good low-temperature flexibility, but the rigid crystalline domains control its elastomeric qualities and thermal resistance [4]. Consequently, it exhibits exceptional mechanical capabilities at elevated temperatures along with remarkable flexibility at low temperatures [5, 6].

Hybridization with inorganic particles is a frequently employed tactic to enhance the mechanical strength and thermal stability of TPEE in order to expand its application. Many micro- and nano-sized particles, including carbon nanotubes, mica, silica, talc, clays, and fly ash, have already been utilized as filler in recent years to enhance the intrinsic qualities of TPEE [7-12]. According to the published results, composite technology works incredibly well to strengthen and increase the stability of TPEE. Because of its exceptional mechanical and thermal properties, graphene Nano sheets or Nano platelets a relatively new type of carbonaceous material have garnered a lot of attention recently [13].

As a result, they are regarded as the reinforcement of the next generation for creating polymer composites with exceptional qualities or

unexpected performance [14]. Several types of graphene-filled epoxy composites, including TPEE ones, have been effectively created thus far [15]. On the TPEE/RGO composites, Paszkiewicz and colleagues [11,12,16] have carried out some excellent research. They created graphene oxide filled poly (trimethyl terephthalate-block-tetramethylene oxide) copolymer composites by using in situ polymerization, and they discovered that the graphene oxide particles could efficiently raise the yield stress and Young's modulus of TPEE. However, there has not been much research done on graphene filled TPEE systems up to this point. Thus, the structure-property relationships of TPEE/graphene composites, particularly the TPEE reinforcement mechanisms, are still deserving of deep study. This study examined the mechanical and viscoelastic properties of TPEE composites containing graphene. Through modeling techniques, the relationship between the mechanical strength of TPEE composites and the surface modification of graphene oxide was investigated, and the reliance of viscoelasticity on phase adhesion was subsequently established. This work's primary goal is to offer a potential method for creating TPEE/ graphene nanocomposites with adjustable characteristics.

In the present work thermoplastic polyester elastomer (TPEE) is prepared and studied the highlights of the impact of incorporating graphene oxide Nano sheets (RGO) on morphological, mechanical, and viscoelastic characteristics of thermoplastic polyester elastomer at 0.5%,1.0% and 1.5% composition ranges.

Experimental

Material:

We bought thermoplastic polyester elastomer TRIEL 5437 from Samyang as a commercial product. With poly (butylene terephthalate) (PBT, 51.09 wt.%) as the hard segments and poly (tetra-methylene glycol) (PTMEG, 48.91 wt.%) as the soft segments (molar ratio 28/72, measured by the approach of Nuclear Magnetic Resonance (NMR) [17], it has a number-average molecular weight (Mn) of approximately 36,000. The Nano sized domains of hard PBT segments of TPEE (with an average size of approximately 100 nm) are distributed throughout its continuous soft phase (bright sections on the modulus images are hard phase and dark ones soft one).

Earlier work [5-7] has found similar phase separation structure and phase size scale of TPEE. The graphite oxide preparation process utilized natural graphite flakes (30–70 mm, purity > 99.97%) that were procured from AD-NANO TECHNOLOGIES Pvt. Ltd., India.

After producing graphite oxide powder using a modified Hummers technique, the graphene oxide (RGO) was exfoliated using ultra-sonication [18,19]. TEM images are included in Fig.1. By melt mixing the RGO-containing composites using a Haake Polylab Rheometer at 220 °C and 50 rpm for six minutes, the composites were created. The clean TPEE was additionally treated to maintain the same thermal histories as the composites for improved comparison.

Prior to use, every item was vacuum-dried for a full day. A Haake mini-jet was used to prepare the rectangular specimens (30 mm 5 mm 1 mm) and the dog-bone-shaped specimens (32 mm 4 mm 2 mm). At a cylinder temperature of 220°C, injection pressure of 600 bar and holding pressure of 500 bar were used throughout the injection molding process. The samples including functionalized and pristine RGO particles are henceforth referred to as TPEE-RGO-s and TPEE-RGO, respectively, where s stands for the weight ratio of RGO particles.

Characterizations of structure and morphology

The dispersion state of GNS in the TPEE nanocomposites was examined by using quantitative nano-mechanical mapping mode and electron microscope with a 120 kV accelerating voltage. For the observation, 100 nm-thick micro-tomed sample sections were utilized. An X-ray photoelectron spectroscopy (XPS) system fitted with an Al anode XR50 source running at 200 W was used to examine the microstructure of nanocomposites. At a pressure of less than $3.0x10^{-7}$ mbar, the overview spectra were recorded at 0.05 eV steps with a pass energy of 20 eV. Thermo Avantage Software was used to deconvolute the overlapping peaks, which were associated with the binding energies as C1s, N1s, and O1s signals.

Characterizations of mechanical properties

The tensile characteristics of the TPEE composites were measured using a Universal Testing Machine (ASTM D638) at a crosshead speed of 50 mm min^{-1}

at 25°C. The provided values for strength and modulus are an average of tests conducted on eight different specimens. Using rectangular specimens, the step cycle tensile tests were conducted at room temperature at a stretching rate of 6 mm s^{-1}. The sample was gradually increased to include other strains. The crosshead direction was changed, and the sample strain was reduced at the same crosshead velocity until zero stress was reached once the sample reached the proper strain. Once it reached the next targeted strain, the sample was stretched once more at the same steady crosshead speed. Until the sample fractured, the unloading-reloading cycles were recorded in this procedure (ε = 1, 2, 3, 4, where ε represents the nominal tensile strain). A DMA Q800 analyzer (TA Instruments, USA) in tensile mode was used to perform creep experiments at different temperatures. The tensile tests yielded an applied stress level of 0.5 - 3.0 MPa, which is in the linear region of all samples. It was decided that the testing would last 10 minutes. As a function of time, the creep strain and compliance were noted. For every sample, three rectangular specimens underwent testing.

Findings and Conversation

RGO Dispersion in TPEE Nanocomposites

TEM pictures of the TPEE composite samples containing the two different types of RGO particles are shown in Fig. 1. It is possible to clearly detect the multilayer nano-platelet structure of RGO along with some fragments with lower lateral diameters.

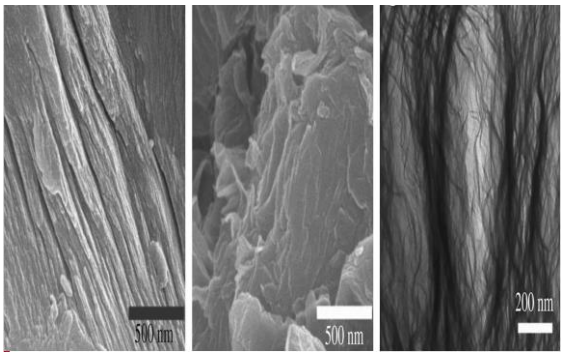

Fig. 1. TEM images of (a) Pure TPEE (b) TPEE-RGO at scale bar of 500 nm (c) TPEE-RGO at scale bar of 200 nm

However, due to their extremely high sizes along the lateral direction (several to tens of micrometers), it is difficult to figure out the distribution difference between these RGO particles in TPEE matrix through TEM observation.

The XPS spectra displayed in Fig. 2 can provide further details on the TPEE and RGO interfacial interactions. The TPEE skeleton's two distinct carbon environments, C-O-C (ether) and O-C O (carboxyl), are represented by the peaks at 286.28 eV (B) and 288.95 eV (D), respectively (Table.1).

Table 1. The XPS spectra of various elastomer composites

Composites	XPS spectra		
			BE (eV)
TPE	A	C-C	284.0±9.3
TPE+0.5%RGO	B	C-O	285.0±7.6
TPE+1%RGO	C	C=O	286.0±5.2
TPE+1.5%RGO	D	O-C-O	288.5±4.9

The multiphase polyester system's interfacial contact levels can be found using the height ratio of these two peaks as a probe [21]. It is evident that TPEE + 1.5% RGO has a greatest B/D value than others i.e., TPEE + 0.5% RGO & TPEE + 1.0% RGO, indicating that RGO's interfacial adhesion to the TPEE matrix can be improved by surface modification.

It is noteworthy that the glass transition temperature (T_g) of the amorphous PTMEG phase of TPEE remains unchanged in the presence of RGO particles suggesting that the presence of RGO particles has no effect on the chain mobility of soft PTMEG. However, there is a clear nucleation effect of GNS on the semi-crystalline PBT phase, as confirmed by an upshift in the crystallization temperature (T_c).

This clarifies that RGO particles interact more strongly with the hard PBT phase of TPEE than they do with the soft PTMEG phase. It should be noted that the limited contrast between the hard and soft phases of TPEE makes it difficult to discern the micro-phase separation structure by TEM inspection [7]. Since the continuous soft phase of the stained samples would cover the dispersion information of RGO, the staining technology is not applicable. Hard PBT phase domains (~100 nm) are much smaller than RGO (along lateral direction) in size, so there might not be any problems with RGO particles' selective localization in the current system.

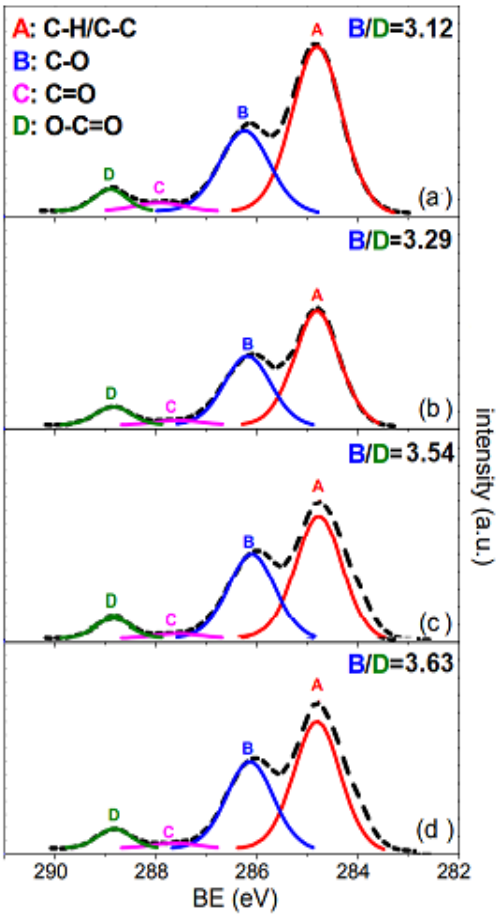

Fig. 2. XPS overview Spectra Carbon signals of (a) TPE, (b) TPE + 0.5%RGO, (C) TPE + 1.0%RGO, (d) TPE + 1.5%RGO samples

Put differently, it makes sense to suggest that, both hard PBT domains and RGO particles are distributed throughout the continuous phase of TPEE. The AFM observation validates this, and it will be covered in more detail later.

TPEE nanocomposites' tensile characteristics

The fact that RGO particles provide strong reinforcement on rubber matrices is commonly known [15]. Table of the Supporting Information provides an overview of the mechanical strength and modulus values for the TPEE composites containing the RGO with various ratios. The maximal strength values of these three composite systems are at 0.1 weight percent RGO loading. Three samples containing (0.5%RGO, 1.0%RGO, and 1.5%RGO samples), are thus used as examples for the mechanical property comparison with plain TPEE.

Fig. 3 displays their respective stress-strain curves. The reinforcement of RGO is confirmed by the composite samples' increased modulus, yield, and tensile strengths compared to the plain TPEE. On the other hand, the increased degree of crystallinity of TPEE matrix

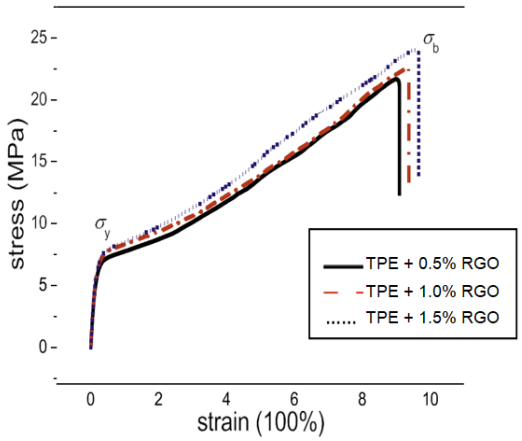

Fig. 3. Stress-strain curves for the composites.

However, the Supporting Information shows, enhanced melting enthalpies in the presence of RGO confirm the increased degree of crystallinity of the TPEE matrix, which also contributes to the improved modulus and strength. When compared to TPEE- RGO -0.5 (7.8 ± 0.4 MPa and 23.8 ± 0.8 MPa), TPEE-RGO -0.5 (7.9 ± 0.4 MPa and 25.6 ± 0.9 MPa) exhibits higher yield and tensile strengths at the identified GNS loadings, confirming that surface modification of RGO is a useful method for promoting load transfer between matrix chain and RGO particles.

In general, filler particles raise system rigidity, which makes composite materials less malleable or ductile than a clean polymer matrix. In contrast to plain TPEE, the three types of TPEE composites exhibit greater elongation at break. It is quite fascinating. Equivalent results have also been observed with GNS [22] or clay tactoids [23] in various different elastomer composites. These investigations ascribed this rise to either enhanced network structure or filler interfacial contact and dispersion. On the other hand, enhanced interfacial adhesion or the development of a better network typically results in a filled polymer composite's higher stiffness and lower plasticity. Because the elongation at break is highly related to the elastoplasticity and viscoplasticity of systems (the

elastic recovery level is approximately 1/4 - 1/5 total deformation after break for the present systems), those explanations may not be applicable to the current systems. PBT domains tend to be enriched on the lateral surface or edges of RGO particles bearing-like structure with RGO, resulting in less friction on the interface between RGO particles and continuous PTMEG phase. RGO particles have a much better affinity to discrete PBT phase than to continuous PTMEG one. This would improve the system's ability to deform, particularly under high strain or stress conditions.

The AFM observation validates the hypothesis of a bearing-like structure. It is possible to clearly observe the RGO platelet fragment embedded in the TPEE matrix, which is consistent with the TEM observation displayed in the inset graph. Because the hard PBT phase has a greater modulus than the soft PTMEG phase, those bright spots represent distinct PBT domains that are abundant on the surface of RGO. It validates the development of a bearing-like structure in composite materials. In tensile tests, the PBT domains may serve as the "bearing ball," promoting elastoplastic deformation. As a result, the composites exhibit more elongation at break than the tidy TPEE. This enrichment effect rises following surface modification of RGO, resulting in a greater concentration of surface enriched PBT domains.

Table 2. The Mechanical and Tensile Strength of various elastomer composites

Composites	Strain	Stress	Ture Strain			
			C		D	
	σ		$\varepsilon_{H,p}$	$\varepsilon_{H,e}$	$\varepsilon_{H,p}$	$\varepsilon_{H,e}$
TPE			0.3±0.07	0.45±0.01	1.4±0.02	0.4±0.01
TPE+0.5%RGO	22.5±2.2	9.0±1.6	0.4±0.11	0.4±0.07	1.6±0.02	0.3±0.01
TPE+1%RGO	23.0±4.1	9.2±0.7	0.47±0.02	0.45±0.08	1.7±0.03	0.32±0.06
TPE+1.5%RGO	24.0±2.2	9.6±0.8	0.48±0.01	0.5±0.07	1.7±0.04	0.25±0.07

Because of the heightened "bearing ball" effect in this instance, TPEE-RGO -0.1 exhibits greater elongation at break than TPEE- RGO -0.1 (Fig. 4). The cyclic tensile tests depict the nominal stress-nominal strain curves during cyclic tensile deformation of neat TPEE and its two composite samples with maximum strain values increased sequentially from 1, 2, 3, and so on up to be broken, further confirm the increased system plasticity in the presence of GNS particles. These curves typically take on this shape when dealing with high content amorphous polymers, since the plastic deformation causes increasingly more residual strain to arise at low stress [24–26].

The composite samples exhibit a higher number of tensile cycles compared to the plain TPEE, suggesting that the inclusion of RGO leads to enhanced plasticity. The composite samples—particularly TPEE-RGO -0.5-require the least amount of work (estimated from cycle area) to reach the same levels of unrecoverable strain. This is explained by the PBT domains' "bearing ball" effect on the RGO surface. Put another way, because of the composites' greater flexibility, the presence of RGO encourages TPEE structural orientation and also favors preserving orientation state in TPEE composites. As a result, those enhanced PBT domains contribute to the increased strength in the tensile direction by acting as a "ball" and shape. Following its return to zero stress, TPEE-RGO -0.5 maintains its higher

Degree of orientation in comparison to clean TPEE further suggesting the composites' enhanced plasticity. Additionally, during tensile tests, the "bearing ball" effect causes an enhanced degree of orientation of the amorphous chain of the PTMEG phase. This is further supported by the plots of the true strains for plastic and elastic materials vs the total true strain in Figure 4.

True strains (εH) for highly deformable materials are defined as ln ð L=L_0, where L/L_0 represents extension ratios. Through experimental testing, the true stress values st ¼ sn ð=L_0 and εH for each cycle are determined (Table.2).

According to Strobl and co-workers' method [26], the maximum true strain in each cycle as the sum of an elastic component εH,e and a plastic component εH,p (determined from the length of

the sample after the stress has been decreased to zero) can then be calculated.

The maximum true strain in each cycle can then be estimated using the Strobl and coworkers' technique [26], which takes the length of the sample-which is obtained after the stress has been reduced to zero—as the sum of the elastic component (εH,e) and the plastic component (εH,p). At strains smaller than point C, some plastic true strain is seen. According to Strobl et al. [26], the breakdown of lamellae connections and lamellae breaking up into blocks inside their copolymer system are the causes of this plastic strain. This is ascribed to the disintegration of the micro phase separation structure of the present TPEE.

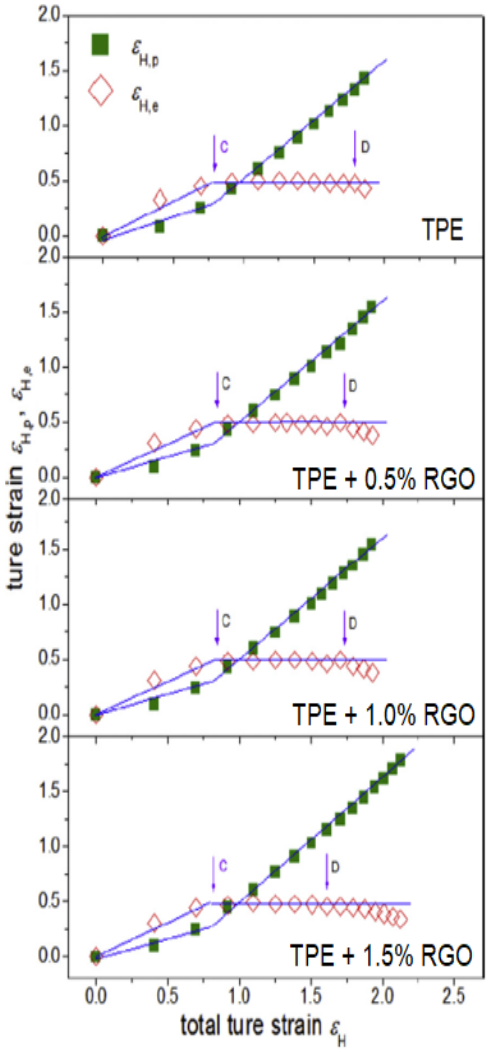

Fig. 4. Plastic and elastic true strains versus the total true strain at the maximum of each cycle of a step cycle tensile test for the neat TPE and its composites.

Since point Cs are nearly at the same strain level in every sample, it is evident that the presence of RGO has negligible effect on the strain sensitivity of this structure. The key points C and D, respectively, are defined by the beginning and end of the plateau, and they correspond to the beginning of the fibrillation processes and chain disentanglement, respectively [25]. As can be shown, point D moves to the lower strain region when RGO is present, particularly for the TPEE-RGO -0.5 sample. This suggests that, as a result of the "bearing ball" effect, surface modification of RGO promotes chain disentanglement and continued phase orientation during deformation with high strain levels.

Stated differently, the barrier effect of RGO is supposed to inhibit chain orientation; on the other hand, PBT domain enrichment on the RGO surface, specifically the formation of a ball bearing structure, can encourage the deformation of soft chain coils and the orientation of the chain during cyclic tensile loading.

The TPEE nanocomposites' creepy behavior

In a linear viscoelastic deformation process, the "ball bearing" structure is not as significant, despite its importance in large-scale or nonlinear deformation. The creep curves for TPEE and its blends are shown in Fig.5. For every sample, the stress level of 2 MPa falls inside the linear zone of deformation (refer to Fig. 3). The creep results at various stress levels are displayed in the Fig.5. It is evident that as compared to the plain TPEE, the two TPEE composites exhibit reduced creep strain levels.

As illustrated in Fig. 5, this tendency is seen over a very long-time span, suggesting that the presence of RGO suppresses chain coil relaxations [27,28] and subsequently delays the viscoelastic deformation of the TPEE matrix. Several other polymer composites containing graphite nano-sheets or RGO have also been shown to exhibit a similar inhibiting effect [29, 30]. This makes sense because, in creep testing, relatively little load is applied, resulting in minimal levels of strain and linear-viscoelastic deformation. Since the large-scale plastic deformation in this instance has not yet occurred, the "ball bearing" structure essentially has no effect on the small-scale

deformation. Consequently, the creep process is dominated by GNS's inhibiting influence on the chain coils.

The strain level of TPEE-RGO -0.5 is observed to be lower than that of TPEE- RGO -1.5, suggesting that improved interfacial adhesion enhances the barrier effect of RGO. It should be noted that, due to improved system rigidity, a somewhat higher degree of crystallinity in the hard PBT phase also contributes to a lower creep level when RGO is present. However, because the soft PTMEG phase is continuous, this effect is not seen. Conversely, Table of the Supporting Information indicates that TPEE-f- RGO -0.5, TPEE- RGO -1.0 and TPEE- RGO -1.5 exhibit nearly equal degrees of crystallinity; however, the former exhibits a lower strain level than the latter. This confirms the obstruction caused by the RGO -chain coil contact as well. An overall evaluation of the creep is provided for each sample using a power law equation created by Findley [31].

It is a linear-viscoelastic deformation. Since the large-scale plastic deformation has not yet occurred, in this instance, the "ball bearing" structure essentially has no effect on the small-scale deformation. Consequently, the creep process is dominated by RGO 's inhibiting influence on the chain coils. The strain level of TPEE-RGO -0.5 is observed to be lower than that of TPEE- RGO -1.5, suggesting that improved interfacial adhesion enhances the barrier effect of RGO. It should be noted that, due to improved system rigidity, a somewhat higher degree of crystallinity in the hard PBT phase also contributes to a lower creep level when RGO is present. However, because the soft phase is continuous, this effect is not seen. Conversely, Table of the Supporting Information (Table.3) indicates that TPEE-RGO -0.5, TPEE- RGO -1.0 and TPEE- RGO -1.5 exhibit nearly equal degrees of crystallinity; however, the former exhibits a lower strain level than the latter. This further supports the RGO -chain coil interface's inhibiting impact. An overall evaluation of the creep is provided for each sample using a power law equation created by Findley [31]:

$$E(t)=\varepsilon_0 þ At^n$$

where A is the transient creep strain amplitude, n is the time exponent, ε(t) is the creep strain at time t, and ε_0 is the instantaneous initial strain. Evidently, the creep of the pure TPEE and its composites can be effectively explained by the Findley model (Fig. 5). The lowered n suggests that the composites would take longer to attain the same creep level as neat TPEE, and the decreased A suggests lower creep levels in the presence of RGO [28, 31], both of which support the barrier function of RGO during TPEE creep.

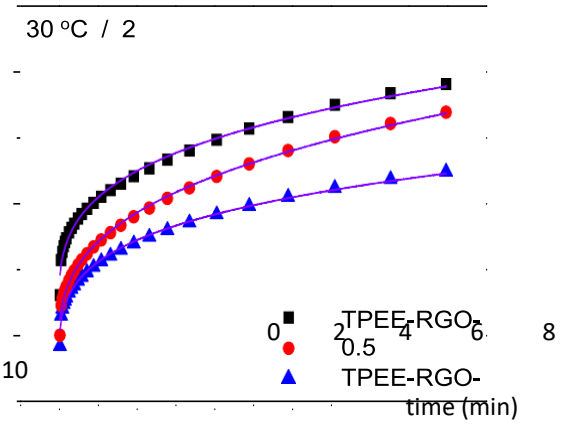

Fig. 5. Findley's model predictions (lines) on the experimental creep data (symbols) of the composites (30 ◦C, 2.0 MPa)

Table 3. Calculated Values of Strain Obtained by Findley's model and Master curves of Elastomer Nanocomposites at 30^{O}C/2MPa.

Composites	Findley's model at 30^{O}C/2MPa	Master curves at 30^{O}C/2MPa	
	Strain	Strain	time (min)
TPE+0.5%RGO	96	90	105
TPE+1%RGO	94	82	105
TPE+1.5%RGO	72	73	105

Conclusions

Melting mixing allows RGO particles to be evenly distributed within the TPEE matrix, and surface modification enhances their interaction with TPEE even more. In TPEE composites, PBT domains tend to be enriched on the surface or edges of RGO particles, producing bearing-like structures with RGO, compared to the soft phase, which has considerably poorer affinity with RGO. In comparison to neat TPEE, this leads to a higher elongation level at the break of composites. The

creation of a bearing-like structure promotes the deformation of soft chain coils and chain orientation during cyclic tensile, which results in an increase in the number of tensile cycles of composites and a reduction in the true strain plateau. But in creep experiments, the RGO barrier effect matters more than the "bearing ball" effect. This is due to the linear viscoelastic nature of creep deformation. Consequently, the presence of RGO inhibits rather than promotes the deformation of the TPEE chain coil.

References

1. G. Holden, N.R. Legge, R.P. Quirk, H.E. Schroeder, Thermoplastic Elastomers, third ed., Hanser Publication, Munich, 2004.
2. N.K. Kaforglou, Thermomechanical studies of semicrystalline polyether-ester copolymers, J. Appl. Polym. Sci. 21 (1977) 543e554.
3. W. Yave, A. Szymczyk, N. Yave, Z. Rosłaniec, Design, synthesis, characterization and optimization of PTT-b-PEO copolymers: a new membrane material for CO2 separation, J. Membr. Sci. 362 (2010) 407e416.
4. Y. Nagai, T. Ogawa, Analysis of weathering of thermoplastic polyester elastomers-I. Polyether-polyester elastomers, Polym. Degrad. Stab. 56 (1997) 115e121.
5. J. Mayumi, A. Nakagawa, K. Matsuhisa, H. Takahashi, H. Takahashi, M. Iijima, Material design and manufacture of a new thermoplastic polyester elastomer, Polym. J. 40 (2008) 1e9.
6. S.Y. Kwak, N. Nakajima, Morphology formation in mixing of co-polyester thermoplastic elastomer (Hytrel) with poly(vinyl chloride) and nuclear magnetic resonance relaxation study on solid structures of the mixture, Macro- molecules 29 (1996) 3521e3524.
7. J.X. Chen, D.F. Wu, X. Yao, Q.L. Lv, J. Wang, Z.S. Li, Nucleation of thermoplastic polyester elastomer composites controlled by silica nanoparticles, Ind. Eng. Chem. Res. (2016), http://dx.doi.org/10.1021/acs.iecr.5b04464.
8. M.S. Sreekanth, S. Joseph, S.T. Mhaske, P.A. Mahanwar, V.A. Bambole, Effects of mica and fly ash concentration on the properties of polyester thermoplastic elastomer composites, J. Thermoplast. Compos Mater 24 (2011) 317e331.
9. J. Bae, S. Lee, B.C. Kim, H.H. Cho1, D.W. Chae, Polyester-based thermoplastic elastomer/MWNT composites: rheological, thermal, and electrical properties,
10. Fiber Polym. 14 (2013) 729e735.
11. O. Aso, J.I. Eguiazabal, J. Nazabal, The influence of surface modification on the structure and properties of a nanosilica filled thermoplastic elastomer, Com-
12. pos Sci. Technol. 67 (2007) 2854e2863.
13. S. Paszkiewicz, A. Szymczyk, X.M. Sui, H.D. Wagner, A. Linares, T.A. Ezquerra,Z. Rosłaniec, Synergetic effect of single-walled carbon nanotubes (SWCNT) and graphene nanoplatelets (GNP) in electrically conductive PTT-block-PTMOhybrid nanocomposites prepared by in situ polymerization, Compos Sci. Technol. 118 (2015) 72e77.
14. S. Paszkiewicz, A. Szymczyk, K. Livanov, H.D. Wagner, Z. Rosłaniec, Enhanced thermal and mechanical properties of poly(trimethylene terephthalate-block- poly(tetramethylene oxide) segmented copolymer based hybrid nano-composites prepared by in situ polymerization via synergy effect between SWCNTs and graphene nanoplatelets, eXPRESS Polym. Lett. 9 (2015) 509e524.
15. E.P. Randviir, D.A.C. Brownson, C.E. Banks, A decade of graphene research: production, applications and outlook, Mater Today 17 (2014) 426e432.
16. H. Kim, A.A. Abdala, C.W. Macosko, Graphene/polymer nanocomposites, Macromolecules 43 (2010) 6515e6530.
17. K.K. Sadasivuni, D. Ponnamma, S. Thomas, Y. Grohens, Evolution from graphite to graphene elastomer composites, Prog. Polym. Sci. 39 (2014) 749e780.
18. S. Paszkiewicz, A. Szymczyk, Z. Sˇpitalský, J. Mosna´ˇcek, K. Kwiatkowski,
19. Z. Rosłaniec, Structure and properties of nanocomposites based on PTT-block- PTMO copolymer and graphene oxide prepared by in situ polymerization, Eur. Polym. J. 50 (2014) 69e77.
20. S.W. Cho, Y.J. Jang, D.M. Kim, T.Y. Lee, D.H. Lee, Y.K. Lee, High molecular weight thermoplastic polyether ester elastomer by reactive extrusion, Polym. Eng. Sci. 49 (2009) 1456e1460.
21. D.C. Marcano, D.V. Kosynkin, J.M. Berlin, A. Sinitskii, Z.Z. Sun, A. Slesarev,

22. L.B. Alemany, W. Lu, J.M. Tour, Improved synthesis of graphene oxide, ACS Nano 4 (2010) 4806e4814.
23. S. Liu, J.Q. Tian, L. Wang, H.L. Li, Y.W. Zhang, X.P. Sun, Stable aqueous dispersion of graphene nanosheets: noncovalent functionalization by a polymeric reducing agent and their subsequent decoration with Ag nano- particles for enzymeless hydrogen peroxide detection, Macromolecules 43 (2010) 10078e10083.
24. K.K. Sadasivuni, D. Ponnamma, B. Kumar, M. Strankowski, R. Cardinaels,
25. P. Moldenaers, S. Thomas, Y. Grohens, Dielectric properties of modified graphene oxide filled polyurethane nanocomposites and its correlation with rheology, Compos Sci. Technol. 104 (2014) 18e25.
26. E. Sainz-García, F. Alba-Elías, R. Múgica-Vidal, A. RGOnza´lez-Marcos, Enhanced surface friction coefficient and hydrophobicity of TPE substrates using an APPJsystem, Appl. Surf. Sci. 328 (2015) 554e567.
27. Z.H. Tang, L.Q. Zhang, W.J. Feng, B.C. Guo, F. Liu, D.M. Jia, Rational design of graphene surface chemistry for high-performance rubber/graphene composites, Macromolecules 47 (2014) 8663e8673.
28. K. Haraguchi, R. Farnworth, A. Ohbayashi, T. Takehisa, Compositional effects on mechanical properties of nanocomposite hydrogels composed of poly(N,N- dimethylacrylamide) and clay, Macromolecules 36 (2003) 5732e5741.
29. Z.G. Wang, Y.H. Niu, G.H. Fredrickson, E.J. Kramer, Y.W. Shin, F. Shimizu,
30. F. Zuo, L.X. Rong, B.S. Hsiao, G.W. Coates, Step-cycle mechanical processing of gels of sPP-b-EPR-b-sPP triblock copolymer in mineral oil, Macromolecules 43 (2010) 6782e6788.
31. F. Deplace, Z.G. Wang, N.A. Lynd, A. Hotta, J.M. Rose, P.D. Hustad, J. Tian,H. Ohtaki, G.W. Coates, G.W. Shimizu, K. Hirokane, F. Yamada, YF. Shin,L.X. Rong, J. Zhu, S. Toki, B.S. Hsiao, G.H. Fredrickson, E.J. Kramer, Processing- structure-mechanical property relationships of semicrystalline polyolefin-based block copolymers, J. Polym. Sci. Part B Polym. Phys. 48 (2010) 1428e1437.
32. R. Hiss, S. Hobeika, C. Lynn, G. Strobl, Network stretching, slip processes, and fragmentation of crystallites during uniaxial drawing of polyethylene and related copolymers: a comparative study, Macromolecules 32 (1999) 4390e4403.
33. H.Y. Liu, L. Yin, D.F. Wu, Z. Yao, M. Zhang, C. Chen, P.F. Fu, J. Qin, Mechanical properties and creep behavior of poly(trimethylene terephthalate)/meso- porous silica composites, Polym. Compos 36 (2015) 1386e1393.
34. Z. Yao, D.F. Wu, C. Chen, M. Zhang, Creep behavior of polyurethane nano- composites with carbon nanotubes, Compos Part A-Appl S 50 (2013) 65e72.
35. L.C. Tang, X. Wang, L.X. RGOng, K. Peng, L. Zhao, Q. Chen, L.B. Wu, J.X. Jiang,
36. G.Q. Lai, Creep and recovery of polystyrene composites filled with graphene additives, Compos Sci. Technol. 91 (2014) 63e70.
37. Y. Wang, Y.X. Cheng, J.X. Chen, D.F. Wu, Y.X. Qiu, X. Yao, Y.N. Zhou, C. Chen, Percolation networks and transient rheology of polylactide composites con-taining graphite nanosheets with various thicknesses, Polymer 67 (2015) 216e226.
38. W.N. Findley, D.B. Peterson, Prediction of long-time creep with ten-year creep data on four plastic laminates, Proc. ASTM 58 (1958) 841e855.